Reconstitution of a prokaryotic minus end-tracking system using TubRC centromeric complexes and tubulin-like protein TubZ filaments

Gero Fink and Jan Löwe[1]

Medical Research Council Laboratory of Molecular Biology, Cambridge CB2 0QH, United Kingdom

Edited by Joe Lutkenhaus, University of Kansas Medical Center, Kansas City, KS, and approved February 25, 2015 (received for review December 11, 2014)

Segregation of DNA is a fundamental process during cell division. The mechanism of prokaryotic DNA segregation is largely unknown, but several low-copy-number plasmids encode cytomotive filament systems of the actin type and tubulin type important for plasmid inheritance. Of these cytomotive filaments, only actin-like systems are mechanistically well characterized. In contrast, the mechanism by which filaments of tubulin-like TubZ protein mediate DNA motility is unknown. To understand polymer-driven DNA transport, we reconstituted the filaments of TubZ protein (TubZ filaments) from *Bacillus thuringiensis* pBtoxis plasmid with their centromeric TubRC complexes containing adaptor protein TubR and *tubC* DNA. TubZ alone assembled into polar filaments, which annealed laterally and treadmilled. Using single-molecule imaging, we show that TubRC complexes were not pushed by filament polymerization; instead, they processively tracked shrinking, depolymerizing minus ends. Additionally, the TubRC complex nucleated TubZ filaments and allowed for treadmilling. Overall, our results indicate a pulling mechanism for DNA transport by the TubZRC system. The discovered minus end-tracking property of the TubRC complex expands the mechanistic diversity of the prokaryotic cytoskeleton.

cytoskeleton | tubulin homologue | DNA segregation

Eukaryotes use microtubules for the segregation of replicated DNAs during the fundamental processes of mitosis and meiosis (1). Some prokaryotes use mitosis-like machineries based on different cytomotive filament systems to maintain and segregate plasmid DNA (2, 3). For example, the ParMRC actin-like system, composed of ATPase protein ParM, adaptor protein ParR, and centromeric DNA *parC*, pushes plasmids to the cell poles by insertional elongation of bipolar ParM spindles, leading to efficient DNA transport and segregation (4–6).

Bacillus thuringiensis (7), *Bacillus anthracis* (8), and *Bacillus cereus* (9) maintain their large, low-copy-number virulence plasmids using *tubZRC* loci. *TubZRC* loci encode the tubulin-like GTPase protein TubZ, adaptor protein TubR, and *tubC* centromeric DNA repeats, which are located directly upstream of the *tubZ* and *tubR* genes on the plasmids.

For *B. thuringiensis* pBtoxis plasmid, it has been shown that the TubZRC maintenance system (referred as "TubZRC") functions via TubZ filaments whose formation and dynamics are both essential for plasmid stability (10). However, TubZRC alone maintains synthetic plasmids only under artificial selective pressure (7, 11), and replication of pBtoxis occurs without the dnaA-box but not without TubZRC, prompting others to propose a role for the TubZRC system in plasmid replication (12). In vitro, TubZ assembles into two- and four-stranded polymers (13–16), and structural studies suggested that the centromeric TubRC complex forms a ring-like structure (17), interacting with the long C-terminal TubZ extensions (18). Thus, it was proposed that the TubRC complex tracks growing ends of TubZ filaments in analogy to the centromeric complex that follows growing filament ends of the actin-like partitioning systems (5, 6, 19). In bulk assays, TubRC has been reported to enhance TubZ filament formation, possibly indicating a switch in dynamic behavior (17, 20).

To uncover how TubR protein and *tubC* DNA harness TubZ filament dynamics for DNA transport, we probed the ability of the three TubZRC components encoded on plasmid pBtoxis of *B. thuringiensis* to self-organize in vitro. We used exclusively untagged, full-length proteins, and molecules were labeled with small chemical dyes for detection. Single-filament dynamics of TubZ have not been described before in vitro. Hence, we first characterized growth and shrinkage of individual filaments, because treadmilling has been described for TubZ filaments in cells (10), in contrast to the dynamic instability that is a hallmark of microtubules and ParM filaments (21, 22).

TubZ Filaments Treadmill

Dynamic TubZ filaments were imaged using total internal reflection fluorescence (TIRF) microscopy (Fig. 1*A*). In the presence of GTP, TubZ filaments formed rapidly and individual filaments, defined as having two visible ends and homogeneous fluorescence intensity (when not speckle-labeled), displayed directed motion, often interrupted by diffusion across the surface (Fig. 1*B*). If elongation and shrinkage were restricted to distinct ends, then filaments could treadmill across the surface, giving the impression of directed motion. Indeed, individual filaments appeared to elongate from one end only, whereas depolymerization occurred from the other end. Complete depolymerization could be observed as well, but it occurred exclusively from one end. To demonstrate directly that filaments have distinct ends and treadmill, we performed dual-color speckle experiments in which only a small fraction of differently labeled TubZ was spiked into the polymerization mix. Speckle labeling of filaments showed that subunits incorporate at the growing, plus end and leave the filament at the

Significance

Bacteria carry large extrachromosomal circular DNA molecules, called plasmids, that contain specific genes causing virulence and drug resistance. An active molecular machine based on actin- or tubulin-like filaments ensures proper inheritance of these low-copy-number plasmids. Tubulin-like filaments are involved in the maintenance of virulence plasmids in pathogens such as *Bacillus thuringiensis*, *Bacillus anthraxis*, and *Bacillus cereus*. We discovered that filaments of tubulin-like TubZ protein and TubRC centromeric complexes, containing TubR protein and *tubC* DNA, encoded on plasmid pBtoxis, self-assemble into a prokaryotic minus end-tracking system. Filament depolymerization and processive TubRC binding to shrinking minus ends cause directed DNA motility, most likely through pulling forces.

Author contributions: G.F. and J.L. designed research; G.F. performed research; G.F. analyzed data; and G.F. and J.L. wrote the paper.

The authors declare no conflict of interest.

This article is a PNAS Direct Submission.

Freely available online through the PNAS open access option.

[1]To whom correspondence should be addressed. Email: jyl@mrc-lmb.cam.ac.uk.

This article contains supporting information online at www.pnas.org/lookup/suppl/doi:10.1073/pnas.1423746112/-/DCSupplemental.

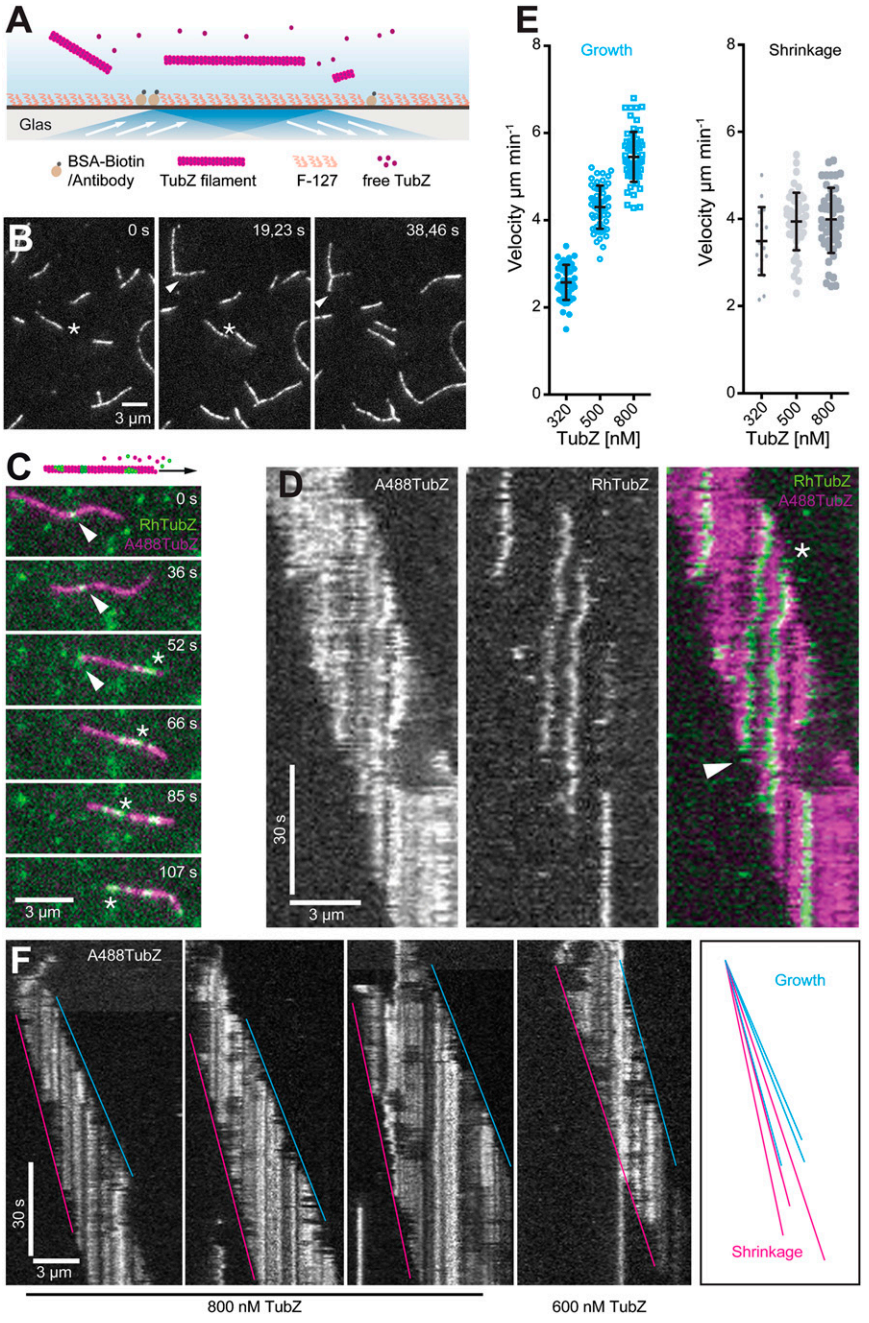

Fig. 1. TubZ filaments treadmill. (*A*) Diagram of the experimental TIRF microscopy setup. TubZ filaments (magenta) were labeled with Atto488 (A488TubZ) or rhodamine (RhTubZ). The glass surface was coated with Pluronic F127, BSA, and antibiotin goat Ig. Filaments were kept in the vicinity of the surface using crowding agent methylcellulose. Ig antibiotin was present in the microscope assay because it was used to immobilize centromeric complexes in later experiments (Fig. 3). Although not required here, we found they improved observation of filaments close to the surface likely by nonspecific interaction. (*B*) Images of speckled A488TubZ filaments gliding (asterisks) and annealing (arrowheads). (*C*) Time-lapse images of dual-color, speckle-labeled filaments demonstrating treadmilling. Individual TubZ molecules (green, arrowheads) remain stationary relative to the filament's motion (magenta) but move when the filament is approximately stationary (asterisks). (*D*) Kymographs of a treadmilling speckled filament. The filament grows to the right and disassembles from the left. RhTubZ molecules incorporate at the growing plus end (asterisk) and leave at the shrinking minus end (arrowhead). (*E*) Scatter plots of growth and shrinkage rates at different TubZ concentrations. Bars represent SD and mean. Growth depends on the TubZ concentration, ranging from 2.57 ± 0.4, to 4.3 ± 0.49, to 5.45 ± 0.57 (mean ± SD, µm·min^{-1}) with $n = 46$, $n = 55$, and $n = 63$. In contrast, shrinking is concentration-independent at 3.49 ± 0.78, 3.94 ± 0.66, and 3.97 ± 0.75 (mean ± SD, µm·min^{-1}), with $n = 17$, $n = 48$, and $n = 48$ (total of two experiments). (*F*, *Left*) Examples of treadmilling filaments displaying net growth at 800 nM TubZ (three panels on left) and one example where shrinkage exceeds growth at 600 nM TubZ (second panel from right). (*F*, *Right*) Lines showing growth and shrinkage rates from the four kymographs (growth rates: 3.3–5.2 µm·min^{-1}, shrinkage: 3.0–3.8 µm·min^{-1}). Note that some background intensity fluctuations were caused by a small operator's light near the microscope.

shrinking, minus end (Fig. 1 *C* and *D* and Movie S1). This behavior is in contrast to microtubules and ParM filaments, which display dynamic instability (21, 22). In TubZ filaments, subunits are lost and added each at one specialized end only, similar to filamentous actin, which treadmills (23).

Quantification of growth rates revealed that elongation depends on the TubZ concentration, whereas shrinkage is independent of free monomer concentration, and hence a zero order intrinsic property of TubZ filaments (Fig. 1 *E* and *F*). Especially at concentrations where growth exceeded shrinkage, filaments rapidly elongated and annealed laterally, forming bundles of different lengths (Fig. 1*B*). Filaments in bipolar bundles treadmilled along each other and separated eventually. Thus, they use each other as tracks (Movie S2). Experiments with differently labeled filament populations clearly demonstrated this behavior: Filaments annealed and treadmilled past each other (Fig. S1 and Movie S3).

TubRC Centromeric Complex Assembles Cooperatively

We then set out to investigate the interaction of TubR with full-length *tubC* DNA consisting of the complete seven iterons, because previous experiments describing the assembly of the centromeric complex used truncated *tubC* (iterons 4–7 only) (12, 17, 18). EMSAs revealed that unlabeled TubR incubated with Atto647-labeled *tubC* 1–7 DNA in motility buffer introduced a full shift at nanomolar concentrations. Analyzing the fraction of bound *tubC* to total *tubC* in dependence of TubR in four EMSA experiments using a one-site binding model with Hill coefficient revealed an apparent K_d of 10.9 nM (Fig. 2*A*). The Hill coefficient obtained is 1.9, indicating cooperative binding behavior of TubR to *tubC*. The cooperativity of adaptor protein to centromeric DNA binding reinforces the similarity in adaptor complex structures observed between the TubZRC system and ParMRC, both forming helical protein oligomers on the DNA

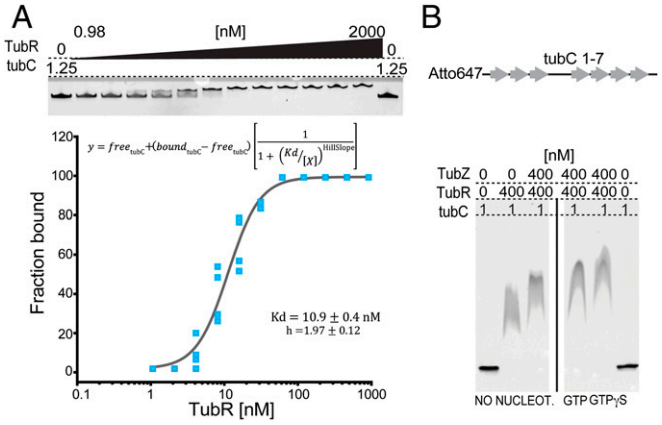

Fig. 2. Interaction of TubR and TubZ with full-length *tubC*. (*A*) EMSA gel picture of Atto647*tubC* 1–7 (as depicted in *B*), interacting with TubR after a 10-min electrophoresis run. TubR concentrations are a twofold serial dilution from 2,000 to 0.98 nM. Most *tubC* is still shifted at about 16 nM TubR. Below is the resulting binding curve, displaying the fraction of *tubC* interacting with TubR at different concentrations, obtained in four independent EMSA experiments, and run for 25 min. The line represents a fit using a one-state binding function with Hill slope. The fit reveals an apparent K_d of 10.9 ± 0.4 nM and a Hill coefficient of 1.97 ± 0.12 (mean ± SE) indicating cooperativity. (*B*) EMSA of Atto647*tubC*. Concentrations for the different reactions are indicated above the gel. A DNA band shift attributable to TubR binding occurs at saturation. (*Lower Right*) TubZ addition reveals an extra shift indicative of TubZ binding, with some additional influence from polymerization-inducing nucleotide (nucleot.).

(6, 17). Highly specific binding of TubR to fluorescently labeled *tubC* was confirmed by an EMSA that included nonspecific control DNA (Fig. S2*A*). Moreover, EMSA showed that the readily assembled centromeric TubRC complex bound nonpolymerized TubZ, as indicated by a super shift (Fig. 2*B* and Fig. S2*B*), which is in agreement with previous reports using shorter *tubC*.

TubRC Tracks the Shrinking Minus End

We next asked if the assembled TubRC complex binds to, and is transported by, TubZ filaments. Indeed, labeled *tubC* DNA showed directed motility in the presence of TubZ and TubR (Movie S4). Importantly, we then found with labeled proteins that the centromeric TubRC complexes bound preferentially to shrinking ends of TubZ filaments (Figs. 3 *A* and *B* and 4*A* and Movies S5 and S6). In addition, transient diffusive binding events occurred along the sides of TubZ filaments. However, *tubC* signals never marked the growing ends. Using the speckled nature of the labeling, these experiments clearly showed that TubRC tracks the minus ends, because speckles disappeared once they encountered a TubRC complex. Bipolar TubZ filament structures having DNA coupled to opposing minus ends formed only by chance and did not separate DNA in vitro; instead, they pulled DNA molecules together (Movies S7 and S8).

We then tested if reducing the number of *tubC* iterons affected TubRC localization and transport. Truncated *tubC* (iterons 1–3) still displayed minus end-specific tracking (Fig. S4 and Movie S9). However, TubRC binding events were reduced. Only 28.1% (of 32 filaments) carried a persistent *tubC* (iterons 1–3) signal, whereas 71.4% (of 42 filaments) carried *tubC* (iterons 1–7).

Our experiments indicated that the centromeric TubRC complex requires full-length *tubC* (iterons 1–7) for efficient filament binding, most likely by providing the maximum number of TubR molecules.

TubRC Does Not Induce Insertional Polymerization

During these experiments, it became obvious that dynamic filaments formed faster in the presence of full-length TubRC. We therefore investigated if binding of TubRC modulated the rate of filament shrinking. Measuring the motion of TubRC signals at

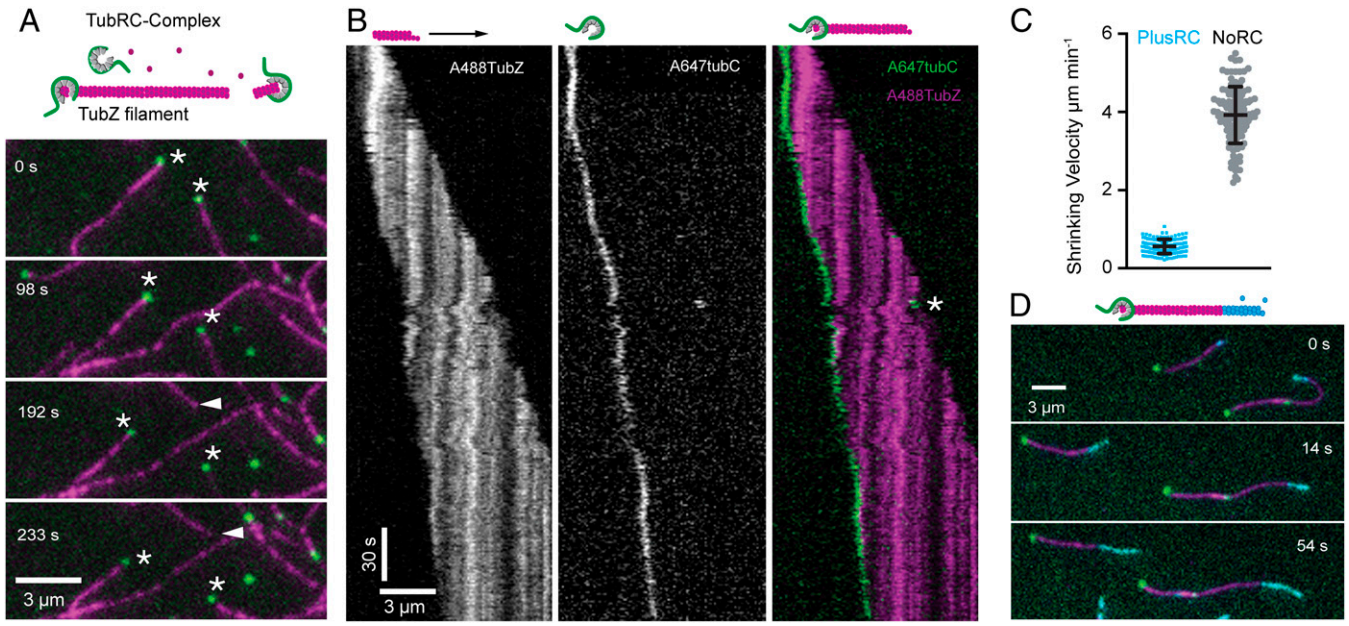

Fig. 3. Processive minus end tracking of TubZ filaments by TubRC. (*A*) Atto647TubRC (green) interacting with A488TubZ filaments (magenta). Dual-color images of TubRC bound to and following shrinking minus ends (asterisks) and not the plus ends (arrowhead) of TubZ filaments are shown. (*B*) Multichannel kymographs illustrating processive minus end tracking of TubRC. The filament emanated from TubRC (arrow) while treadmilling across the surface. TubRC tracked the minus end, as indicated by the loss of speckles, but also shows some transient lateral binding (asterisk). More examples are shown in Fig. S3*A*. (*C*) Scatter plots of TubRC minus end-tracking velocities (0.495 ± 0.182 µm·min^{-1}, mean ± SD; n = 152; two experiments) compared with pooled minus end shrinking rates from Fig. 1*E*. (3.883 ± 0.73 µm·min^{-1}, mean ± SD; n = 113). TubZ filament shrinking was greatly reduced when TubRC was bound (also Fig. S4*B*). (*D*) Polarity-marked TubZ filaments. Filaments were composed of seeds (magenta) and extensions (cyan). Time-lapse fluorescence micrographs of polarity-marked filaments showed filament extension occurring only at ends not bound by the A647TubRC complex. Another example is shown in Fig. S3*B*.

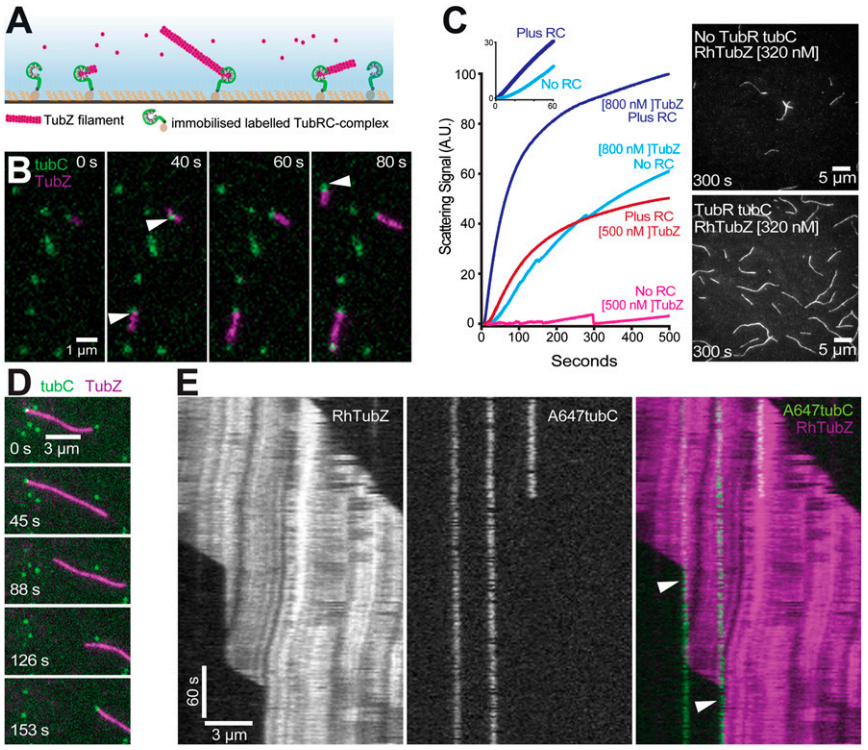

Fig. 4. TubRC complexes seed TubZ filaments and bind to preformed filaments. (*A*) Schematic diagram of labeled TubZ filaments (magenta) seeded by and growing off antibody-immobilized Atto647TubRC complexes (green). (*B*) Time-lapse, dual-color images of A488TubZ filaments that assembled preferentially at A647TubRC sites (arrowheads). (*C*, *Left*) Bulk light scattering experiment of unlabeled TubZ polymers formed in the presence or absence of TubRC. (*C*, *Inset*) Shorter nucleation-dominated lag phase was observed with TubRC (intensity-normalized). Below a critical concentration, TubZ polymers formed only in the presence of TubRC. (*C*, *Right*) Same effect was observed with fluorescently labeled TubZ and TubRC in TIRF experiments (images of RhTubZ filaments shown). A.U., arbitrary units. (*D*) Micrograph of a TubZ filament releasing from and reattaching to different individual surface-bound TubRC complexes. (*E*) Dual-channel kymographs illustrating the persistence of TubRC complexes binding to a minus end, confirming the processive minus end-tracking behavior. The filament treadmilled over surface-bound TubRC complexes from left to right and stalled when an individual TubRC encountered the minus end (arrowheads). Note that speckles leave the filament faster when not bound to TubRC. Some *tubC* signals along the path of the TubZ filament bleached during the observation.

TubZ filament minus ends revealed an approximately sevenfold reduction in shrinkage compared with TubZ filaments alone (Fig. 3*C*). Binding of both truncated (iterons 1–3) and full-length (iterons 1–7) TubRC allowed for slow depolymerization and did not inhibit treadmilling. This effect explained the previously suggested stabilization effect of TubRC on filament formation (17, 20). To check that the measured reduction in shrinkage was not caused by TubZ filament growth facilitated by bound TubRC, filaments were sequentially grown using differently labeled TubZ monomers, whereas TubR and *tubC* concentrations were kept constant. Clearly, new TubZ monomers incorporated only at the filament ends that were free of TubRC (Fig. 3*D*, Fig. S3*B*, and Movie S10). We concluded that the centromeric complex does not drive insertional polymerization; it merely tracks minus ends while reducing the rate of monomer loss.

TubRC Supports the Seeding of TubZ Filaments

The finding that TubRC bound monomeric TubZ molecules in EMSAs (Fig. 2*B*) raised the possibility that the centromeric complex could initiate filament growth by seeding (assisted nucleation). To test for seeding, we followed filament formation on immobilized TubRC complexes (Fig. 4*A*). In time-lapse movies, we observed that filaments formed and emanated first and mostly at sites of individual centromeric TubRC complexes (Fig. 4*B* and Movies S11 and S12). Filaments sometimes detached after nucleation from surface-bound TubRC and treadmilled until the minus end encountered a new TubRC to which the end adhered and then depolymerized with a slower rate (Fig. 4 *D* and *E* and Movie S13). During the first few minutes, 76.22 ± 1.89% (mean ± SD; n = 211, obtained in three experiments) of filaments originated with one end from a TubRC site. Interestingly, short filaments displayed initial nodal swiveling on TubRC sites, an indication of a single attachment point (24) (Movies S11 and S12). These experiments suggested that the centromeric complex, probably through its large number of TubZ monomer-binding sites, recruits TubZ subunits to form a seed from which growth occurs. They also confirmed the specificity and minus end residency of the centromeric complex seen previously with nonimmobilized TubRC (Movies S5–S8).

To support further the notion of TubRC-mediated nucleation, we performed light scattering experiments with unlabeled proteins. First, we aimed to detect the stabilizing effect of TubRC complexes on TubZ polymerization below the concentration where TubZ alone shows a detectable light scattering signal (below the critical concentration of TubZ). Indeed, only in the presence of TubRC complexes was a clear signal measurable (Fig. 4*C*). The increase in filament formation could have been caused either by the reduction in depolymerization yielding longer filaments or by increased nucleation giving more filaments. To discriminate between these two possibilities, polymerization of TubZ in the presence and absence of TubRC was monitored above the critical concentration. Again, TubRC promoted filament formation, as indicated by the increased signal. Additionally, we detected a reduced nucleation-dominated initial lag phase (Fig. 4*C*, *Inset*). The initial slope when plotting scattering signal vs. time on a double-logarithmic scale yields the number of steps required for the formation of a growing filament (19, 25). Indeed, TubRC changed the slope of the initial polymerization signal, further supporting the finding that TubZ filaments nucleate by fewer steps when TubRC is present than with TubZ alone (Fig. S5). Thus, TubRC controls TubZ filament assembly in vitro, recruiting individual TubZ subunits and reducing depolymerization, and both activities lead to more TubZ in filaments. That these activities require full-length *tubC* is supported by previous light scattering experiments (17). Because of the seeding activity, filaments could first originate from the centromeric plasmid DNA in cells, rather than the plasmid hopping on and off, obviating a need for a search-and-capture mechanism of filament engagement.

Discussion

We have shown that tubulin-like TubZ filaments are one-dimensional motors, most likely driving directed DNA transport by pulling on DNA. Transport of the centromeric TubRC complex is accomplished by its property to recognize and bind to shrinking minus ends persistently rather than the growing plus ends. As a result of depolymerization, filaments exert force from the minus end, pulling on TubRC while treadmilling. Force generation

requires that the filaments experience resistance to movement through viscosity, surface binding, or interaction with other filaments as occurring in vitro.

TubR has been reported previously to bind to the long C-terminal tails of TubZ (18). We therefore propose that the filament minus ends expose multiple TubZ C-terminal tails as suggested for the four-stranded TubZ filament (16). Unfortunately, the tails were not resolved in recent EM TubZ filament reconstructions (16), but it can be deduced from the structures that the filaments will most likely have TubR-binding tails exposed at one end only. The accessibility of TubZ tails for TubRC centromeric complexes at one end of the filament assumes that the tails also bind along the filament, latching onto subunits further up as has clearly been seen in phage TubZ (PhuZ) protofilament crystal structures (26, 27). In accordance with competitive TubZ tail binding between the filament lattice and TubRC, we have observed lateral interaction of TubRC with filaments. Lateral events are short-lived compared with minus end binding, the only place where there is no competition for the tails by the TubZ filament lattice. Because assembled TubRC also has multiple binding sites for the minus end TubZ tails, it can stay attached during shrinkage, although the exact mechanism of this end-binding behavior remains to be elucidated.

TubZ tails binding along the filament would also explain the extraordinary stability of the plus ends that apparently do not depolymerize in our experimental conditions. The subunits at the plus end have additional contacts with the filament that those subunits at the minus end do not have because their tails do not bind to the filament. However, clearly, more studies of TubZ filaments and their attachment to TubRC are required to assign polarity, recognizing one particular TubZ filament end as the shrinking minus end and the other as the plus end.

The behavior of TubZRC described here is unexpected because of its structural similarities to the actin-like partitioning systems (17). The centromeric complex of the ParMRC actin-based partitioning system accelerates growth of filaments by binding at the growing (barbed) end, catalyzing insertion of polymer subunits (5). TubZRC does not exclusively form bipolar spindles, as does ParMRC, because there is no dynamic instability making unipolar assemblies unstable. The stable formation of unipolar attachments of TubZ filaments to TubRC means that there is no self-selection for the formation of productive bipolar spindles that push DNAs away from each other, as in the ParMRC system (4–6, 19, 21). Thus, TubZRC alone cannot separate DNAs; it will cluster DNA when forming bipolar filament structures.

The in vivo observation of treadmilling TubZ filaments in *Bacillus* cells that bend around the cell poles (10) seems to support the notion of a pulling mechanism for transport instead of pushing by bipolar spindle structures, because at least one property we observed in vitro, treadmilling, has been observed in vivo. However, it remains to be seen how cells make use of the newly discovered end-tracking activity in the TubZRC system or if it is only part of a more complex mechanism. More complex mechanisms might involve that the initial growing end is captured to a cellular structure, which then contributes to pulling of DNA when disassembling. Additional components similar to organizing centers, spindle poles that anchor filaments as suggested for the PhuZ-based phage centering system (28), or other regulators may be required (29). One possibility for an anchor could be the nucleoid, and it has been noted that another gene, downstream of TubZRC, tubY (pBt158 on pBtoxis), might have DNA-binding activity and hence might be a candidate for this requirement (20). Alternately, at high intracellular TubZ concentrations, net growth could prevail, meaning a pushing mechanism is possible in principle. We think a pushing mechanism alone is unlikely because, otherwise, there would have been no reason to conserve minus end tracking during the evolution of this system.

As a last possibility, TubZRC might not even separate DNA, like the actin systems, and, for example, might support efficient replication by shuffling the plasmid through the cell.

In conclusion, we report, to our knowledge, the first in vitro reconstitution of transport by depolymerizing filaments of a bacterial filament system. The property to track shrinking cytomotive filament ends to couple pulling forces to DNA has so far only been described for the eukaryotic kinetochore complex (30). In vitro, kinetochores processively track depolymerizing microtubules using biased diffusion and multiple binding sites (31), and they also reduce shrinking rates (32).

Our findings provide further evidence of the emerging functional richness of the bacterial cytoskeleton.

Materials and Methods

Protein Expression and Purification. A detailed description is provided in *SI Materials and Methods*. Briefly, *B. thuringiensis* TubZ and TubR fused to intein- and sumo-tags, respectively, were recombinantly expressed in *Escherichia coli*. Proteins were cleaved on the affinity column, eluted, and further purified by ion exchange and size exclusion chromatography. For TubZ, this purification procedure was combined with a polymerization/depolymerization cycle (below) yielding functional TubZ. All steps were quickly performed on ice or at 4 °C unless stated otherwise, because proteolysis of disordered tails, especially for TubZ, posed a challenge. Correct molecular weights of purified proteins were confirmed by mass electrospray spectrometry.

Polymerization and Labeling of TubZ. Filaments were labeled using surface-exposed lysine residues by amine-conjugated Atto or rhodamine dyes (Jena Bioscience or Pierce) following a combination of the manufacturers' protocols and labeling procedures for tubulin (33). In brief, after affinity purification or gel filtration, TubZ was diluted in buffer-L [50 mM K-Hepes (pH 8), 200 mM KCl, 1 mM ethylenediaminetetraacetic acid (EDTA), 0.2 mM *tris*(2-carboxyethyl)phosphine (TCEP)] at a 1 (protein):1.5 (dye) ratio and polymerized at room temperature by addition of 5 mM $MgCl_2$ and 2 mM GTP during the labeling reaction (30 min to 1 h). The reaction was quenched using an equal volume of buffer-L, supplemented with 100 mM K-glutamate instead of 200 mM KCl; again, 2 mM GTP was added. After 1 min, TubZ filaments were separated from free dye and nonpolymerized protein by centrifugation at 100,000 × *g* for 20 min over a 40% (vol/vol) glycerol cushion (buffer-L with 100 mM K-glutamate) using a Beckman TLA 100 rotor. After aspirating the supernatant, the pellet was rinsed and resuspended in buffer-R [50 mM K-Hepes (pH 7.5), 150 mM K-glutamate, 2 mM EDTA, 0.2 mM TCEP] using a Dounce homogenizer. Subsequently, filaments were depolymerized at 37 °C until the solution was clear. Protein aggregates were removed by a second spin at 200,000 × *g* for 10 min. After the depolymerization, the protein-to-label ratio was determined using a NanoDrop ND-1000 Spectrophotometer, and the concentrations were calculated using calculated extinction coefficients.

In Vitro Single-Molecule and Polymerization Assays. Microscope chambers were constructed of silanized coverslips as described previously (34, 35). Channels were incubated with antibiotin antibody (Sigma) in phosphate-buffered saline (PBS) for 3 min, washed with 40 μL of PBS, and blocked for 30 min with 1% Pluronic F127 (Sigma) in PBS. Channels were then rinsed with 40 μL of PBS and 60 μL of buffer-MB [150 mM K-glutamate, 50 mM K-Hepes (pH 7.5), 5 mM $MgCl_2$, 1 mM EDTA, 0.2 mM TCEP, 0.01% Tween 20, 3.5 mg·mL^{-1} BSA]. Before imaging, channels were equilibrated with 20 μL of buffer-MB, containing antifade (40 mM glucose, 40 μg·mL^{-1} glucose oxidase, 16 μg·mL^{-1} catalase, 1 mM DTT). Labeled TubZ alone and with TubRC in buffer-MBG (buffer MB plus antifade, 0.5 mM GTP, 0.6% methycellulose [400 cP (centipoise)]) was added in two subsequent steps of 10 μL while acquiring images. Atto488-labeled TubZ at different concentrations (labeled 1:18 unlabeled) was spiked with 6.4 nM rhodamine-labeled TubZ (labeled 1:7 unlabeled) in speckle experiments. For end tracking, 8 nM unlabeled TubR and 20 pM Atto647-labeled *tubC* were *tubC* used. Labeling of *tubC* is described in *SI Materials and Methods*. Continuous treadmilling of TubZ filaments along the surface occurred on antibiotin antibody-treated surfaces and was easier to follow compared with surfaces without antibody. On non–antibody-treated surfaces, only filament bundles remained long enough in the field of view to track growing and shrinking ends. For polarity-marked TubZ filaments, rhodamine-labeled TubZ filaments were grown in buffer-MBG from Atto647-labeled TubRC complexes. Then, a wash containing Atto488-labeled TubZ, while imaging, replaced nonpolymerized rhodamine-labeled TubZ. The concentrations of TubRC were held constant. For immobilized TubRC complexes, first surfaces were coated with antibodies against biotin and blocked, then biotinylated and Atto647-labeled *tubC* in TE (Tris-EDTA) buffer (50–200 pM) was allowed to bind for 10–15 min; this was followed by

washes to remove unbound *tubC*. Channels were then rinsed with 60 μL of buffer-MB (containing 50 or 150 mM K-glutamate), followed by addition of TubR in buffer-MB at a concentration of 100 nM for 5 min. Finally, polymerization solution buffer-MBG (in 0.2–0.6% methycellulose) was added containing monomeric, labeled TubZ from 320 nM to 800 nM and nonlabeled TubR at 100 nM. Imaging commenced immediately after that procedure.

Imaging and Analysis. Labeled TubZ filaments and Atto647-labeled *tubC* were visualized at 24 ± 1 °C using an inverted fluorescence microscope (Nikon) with a Nikon 100×, 1.49-N.A., oil, APO TIRF objective and a back-illuminated EMCCD camera (iXon^{EM+} DU-897E; Andor Technology) controlled by μManager (micro-manager.org/wiki/Micro-Manager). For TIRF illumination, 488-nm and 561-nm lasers (both 150 mW; Coherent Sapphire), as well as 100-mW, 641-nm lasers (Coherent Cube), were used. In multicolor experiments, images were acquired sequentially by switching emission filters between GFP, Cy3, and Cy5 (Chroma Technology Corp.). Image acquisition rates ranged from 1.6 to 0.5 frames per second with exposures of 100 ms. Details of image analysis are found in *SI Materials and Methods*.

Light Scattering. Rapid polymerization reactions were followed using an SX-17MV Stopped Flow Spectrofluorimeter (Applied Photophysics) utilizing 1:1 mixing. Changes in scattered light intensity were followed at 340 nm in a conventional (90°) fluorescence detection mode. TubZ was monitored at 500 nM and 800 nM in the presence of 250 μM GTP in buffer-MB (50 mM K-glutamate) at 23 °C, whereas TubR (400 nM) and *tubC* (1 nM) were kept constant. The obtained signal was normalized by subtraction of the baseline and setting the smallest value of all curves to 0 and the largest value of all curves to 100. For the change in the lag phase, as well as the log–log plot setting, the smallest value to 0 and the largest value to 100 for each curve separately normalized each curve.

EMSA. PCR products were produced from primers, of which one was 5′-conjugated to Atto647NN for *tubC* or to Atto488 for control DNA amplified from the ampicillin resistance of pTXB1 and purified by gel extraction. *TubC* and control DNA at 1 nM (final concentration) were incubated with varying concentrations of TubR and TubZ as indicated, yielding different ratios. Components were incubated for 15 min in 50 μL of standard buffer-MB also used for microscopy but without antifade. Fifteen microliters of the reaction was loaded onto a gel. Protein–DNA complexes were separated on 6% (wt/vol) acrylamide TBE (Tris-Borate-EDTA) gels run for 40 min at 160 V. Atto647-labeled *tubC* was detected using a Typhoon Trio Imager (GE Healthcare). Quantitative EMSA samples were resolved on Criterion (Biorad) 4–16% (wt/vol) TBE gels run at 160 V for 10 min and 25 min. Ten microliters of the reaction mix in standard buffer-MB was loaded. Fractional intensities of starting material *tubC* without TubR and interacting TubR/*tubC* were determined using ImageQuant TL software. For quantitative analysis, the intensity of the band for each lane was corrected manually, subtracting the intensity of the background in front and after each peak. The total signal in each lane was set to 100% to correct for errors in loaded sample volume. The area of unbound *tubC* run to the left and right was used and transferred to each lane to determine the fraction of unbound *tubC* to bound *tubC*. The resulting value was taken as *tubC* bound to TubR. The data were fitted for simplicity to a one site-specific binding model with Hill coefficient using the following equation: $y = free"tubC" + (bound"tubC" - free"tubC")[1/(1+(Kd/[X])\text{^}"HillSlope")]$, where the X variable is the concentration of TubR, for fitting bound and unbound *tubC* were constrained to 100 and 0, respectively, yielding $R^2 = 0.99$.

ACKNOWLEDGMENTS. We thank Christopher H. S. Aylett for help with protein purification, Linda A. Amos and Fusinita van den Ent for discussions, members of the Meindert Lamers group for advice on EMSA, and Chris M. Johnson for help with the light scattering (all from Medical Research Council Laboratory of Molecular Biology). We thank Marija Zanic (Vanderbilt University) for discussions and comments on the manuscript. This work was supported by the Medical Research Council (Grant U105184326) and the Wellcome Trust (Grant 095514/Z/11/Z). G.F. was supported by a Leopoldina postdoctoral fellowship (Grant LPDS 2013-06).

1. Gadde S, Heald R (2004) Mechanisms and molecules of the mitotic spindle. *Curr Biol* 14(18):R797–R805.
2. Gerdes K, Howard M, Szardenings F (2010) Pushing and pulling in prokaryotic DNA segregation. *Cell* 141(6):927–942.
3. Schumacher MA (2012) Bacterial plasmid partition machinery: A minimalist approach to survival. *Curr Opin Struct Biol* 22(1):72–79.
4. Garner EC, Campbell CS, Weibel DB, Mullins RD (2007) Reconstitution of DNA segregation driven by assembly of a prokaryotic actin homolog. *Science* 315(5816): 1270–1274.
5. Gayathri P, et al. (2012) A bipolar spindle of antiparallel ParM filaments drives bacterial plasmid segregation. *Science* 338(6112):1334–1337.
6. Møller-Jensen J, et al. (2003) Bacterial mitosis: ParM of plasmid R1 moves plasmid DNA by an actin-like insertional polymerization mechanism. *Mol Cell* 12(6):1477–1487.
7. Tang M, Bideshi DK, Park HW, Federici BA (2006) Minireplicon from pBtoxis of Bacillus thuringiensis subsp. israelensis. *Appl Environ Microbiol* 72(11):6948–6954.
8. Akhtar P, Anand SP, Watkins SC, Khan SA (2009) The tubulin-like RepX protein encoded by the pXO1 plasmid forms polymers in vivo in Bacillus anthracis. *J Bacteriol* 191(8):2493–2500.
9. Hoshino S, Hayashi I (2012) Filament formation of the FtsZ/tubulin-like protein TubZ from the Bacillus cereus pXO1 plasmid. *J Biol Chem* 287(38):32103–32112.
10. Larsen RA, et al. (2007) Treadmilling of a prokaryotic tubulin-like protein, TubZ, required for plasmid stability in Bacillus thuringiensis. *Genes Dev* 21(11):1340–1352.
11. Ge Y, et al. (2014) A new tubRZ operon involved in the maintenance of the Bacillus sphaericus mosquitocidal plasmid pBsph. *Microbiology* 160(Pt 6):1112–1124.
12. Tang M, Bideshi DK, Park HW, Federici BA (2007) Iteron-binding ORF157 and FtsZ-like ORF156 proteins encoded by pBtoxis play a role in its replication in Bacillus thuringiensis subsp. israelensis. *J Bacteriol* 189(22):8053–8058.
13. Chen Y, Erickson HP (2008) In vitro assembly studies of FtsZ/tubulin-like proteins (TubZ) from Bacillus plasmids: Evidence for a capping mechanism. *J Biol Chem* 283(13): 8102–8109.
14. Anand SP, Akhtar P, Tinsley E, Watkins SC, Khan SA (2008) GTP-dependent polymerization of the tubulin-like RepX replication protein encoded by the pXO1 plasmid of Bacillus anthracis. *Mol Microbiol* 67(4):881–890.
15. Aylett CH, Wang Q, Michie KA, Amos LA, Löwe J (2010) Filament structure of bacterial tubulin homologue TubZ. *Proc Natl Acad Sci USA* 107(46):19766–19771.
16. Montabana EA, Agard DA (2014) Bacterial tubulin TubZ-Bt transitions between a two-stranded intermediate and a four-stranded filament upon GTP hydrolysis. *Proc Natl Acad Sci USA* 111(9):3407–3412.
17. Aylett CH, Löwe J (2012) Superstructure of the centromeric complex of TubZRC plasmid partitioning systems. *Proc Natl Acad Sci USA* 109(41):16522–16527.
18. Ni L, Xu W, Kumaraswami M, Schumacher MA (2010) Plasmid protein TubR uses a distinct mode of HTH-DNA binding and recruits the prokaryotic tubulin homolog TubZ to effect DNA partition. *Proc Natl Acad Sci USA* 107(26):11763–11768.
19. Polka JK, Kollman JM, Mullins RD (2014) Accessory factors promote AlfA-dependent plasmid segregation by regulating filament nucleation, disassembly, and bundling. *Proc Natl Acad Sci USA* 111(6):2176–2181.
20. Oliva MA, Martin-Galiano AJ, Sakaguchi Y, Andreu JM (2012) Tubulin homolog TubZ in a phage-encoded partition system. *Proc Natl Acad Sci USA* 109(20):7711–7716.
21. Garner EC, Campbell CS, Mullins RD (2004) Dynamic instability in a DNA-segregating prokaryotic actin homolog. *Science* 306(5698):1021–1025.
22. Mitchison T, Kirschner M (1984) Dynamic instability of microtubule growth. *Nature* 312(5991):237–242.
23. Wegner A, Isenberg G (1983) 12-fold difference between the critical monomer concentrations of the two ends of actin filaments in physiological salt conditions. *Proc Natl Acad Sci USA* 80(16):4922–4925.
24. Howard J, Hudspeth AJ, Vale RD (1989) Movement of microtubules by single kinesin molecules. *Nature* 342(6246):154–158.
25. Flyvbjerg H, Jobs E, Leibler S (1996) Kinetics of self-assembling microtubules: An "inverse problem" in biochemistry. *Proc Natl Acad Sci USA* 93(12):5975–5979.
26. Aylett CH, Izoré T, Amos LA, Löwe J (2013) Structure of the tubulin/FtsZ-like protein TubZ from Pseudomonas bacteriophage ΦKZ. *J Mol Biol* 425(12):2164–2173.
27. Kraemer JA, et al. (2012) A phage tubulin assembles dynamic filaments by an atypical mechanism to center viral DNA within the host cell. *Cell* 149(7):1488–1499.
28. Erb ML, et al. (2014) A bacteriophage tubulin harnesses dynamic instability to center DNA in infected cells. *eLife* 3:3.
29. Ge Y, et al. (2014) A novel transcriptional activator, tubX, is required for the stability of Bacillus sphaericus mosquitocidal plasmid pBsph. *J Bacteriol* 196(24):4304–4314.
30. Westermann S, et al. (2006) The Dam1 kinetochore ring complex moves processively on depolymerizing microtubule ends. *Nature* 440(7083):565–569.
31. Powers AF, et al. (2009) The Ndc80 kinetochore complex forms load-bearing attachments to dynamic microtubule tips via biased diffusion. *Cell* 136(5):865–875.
32. Umbreit NT, et al. (2012) The Ndc80 kinetochore complex directly modulates microtubule dynamics. *Proc Natl Acad Sci USA* 109(40):16113–16118.
33. Hyman AA (1991) Preparation of marked microtubules for the assay of the polarity of microtubule-based motors by fluorescence. *J Cell Sci Suppl* 14:125–127.
34. Fink G, et al. (2009) The mitotic kinesin-14 Ncd drives directional microtubule-microtubule sliding. *Nat Cell Biol* 11(6):717–723.
35. Gell C, et al. (2010) Microtubule dynamics reconstituted in vitro and imaged by single-molecule fluorescence microscopy. *Methods Cell Biol* 95:221–245.

Supporting Information

Fink and Löwe 10.1073/pnas.1423746112

SI Materials and Methods

DNA Manipulations. Recombinant expression plasmids were designed and constructed following manufacturer's instructions for pTXB1 of the IMPACT Kit (New England Biolabs) and pOPINS (OPPF-UK). The plasmid for the expression of *B. thuringiensis* pBtoxis TubZ was constructed by PCR amplification of the full-length coding sequence (UniProt Q8KNP3) from plasmid pET28-a-TubZH (1). The internal NdeI site within the ORF of TubZ was removed by site-directed mutagenesis, changing CATATG to CATACG, resulting in a silent mutation. Mutagenesis and amplification were performed using KOD polymerase (Novagen) and three different PCR reactions, introducing the leading NdeI site, trailing SapI site, and silent mutation removing the internal NdeI site. The resulting PCR product was cut with NdeI and Sap1 and ligated into the pTXB1 vector, producing plasmid pTXB1-BtTubZ. An N-terminal fusion protein of His_6-Sumo with TubR was constructed using vector pOPINS. The ORF of *B. thuringiensis* pBtoxis TubR (UniProt Q8KNP2) was amplified from pHis17-BtTubR (2) using primers for In-Fusion restriction-free cloning containing recommended extensions to overlap with the plasmid backbone at the multiple cloning site (forward primer: GCGAACAGATCGGTGGT, reverse primer: ATGGTCTAGAAAGCTTTA). Restriction-free cloning was performed using an In-Fusion Kit (Clontech) according to the manufacturer's instructions, resulting in plasmid pOPINS-BtTubR. The correctness of all DNA manipulations described above was confirmed by DNA sequencing.

Protein Expression and Purification. The following recombinant expression constructs were used: (*i*) pTXB1-BtTubZ, expressing unlabeled, C-terminally intein-tagged, full-length TubZ and (*ii*) pOPINS-BtTubR, expressing N-terminally SUMO-tagged, full-length TubR. Expression of TubZ and TubR was carried out in *E. coli* strain C41 (Invitrogen). Cells were grown in 2× YT (yeast/tryptone) broth, supplemented with the requisite antibiotic (100 μg/L ampicillin or 50 μg/L kanamycin), grown at 37 °C, and induced with 1 mM isopropyl β-D-thiogalactoside for 4 h at 37 °C at an OD_{600} between 0.5 and 0.7. Cells were harvested by centrifugation at 4,000 × *g* and resuspended in lysis buffer containing complete protease inhibitor tablets (Roche). They were broken at 25 kpsi, at 4 °C, with a cell disruptor (Constant Systems). The lysate was clarified by centrifugation at 45,000 × *g*, and proteins were then purified by chromatography using an ÄKTA Purifier LC System (GE Healthcare).

TubZ was purified from cleared lysate in [50 mM K-Hepes (pH 7.5), 500 mM KCl, 10 mM EDTA, 0.5 mM TCEP] by chitin-affinity chromatography (New England Biolabs). The column was washed in cleavage buffer containing 1 mM EDTA, 50 mM DTT, and 300 mM KCl. Cleavage was allowed for up to 16 h, and the protein was eluted subsequently. Purity was further improved by anion exchange [5 mL of HiTrap Q HP (GE Healthcare) 50 mM K-Hepes (pH 7.5), 1 mM EDTA, 0.2 mM TCEP, 100–800 mM KCl gradient], followed by size exclusion chromatography [HiLoad Sephacryl S200 16/60 (GE Healthcare), 50 mM K-Hepes (pH 7.5), 200 mM KCl, 1 mM EDTA, 0.2 mM TCEP]. For TubZ only, we further purified the protein after affinity purification and cleavage by a polymerization, centrifugation, and depolymerization cycle at room temperature, yielding protein enriched for polymerization propensity.

TubR protein was purified by chromatography from the cleared cell lysate after centrifugation essentially as described earlier (2). Briefly, TubR proteins were retrieved by nickel affinity chromatography [5 mL HisTrap HP (GE Healthcare), 100 mM Tris·Cl (pH 8.5), 500 mM NaCl, 1 mM EDTA, 3 mM imidazole, 5% (vol/vol) glycerol] in the presence of protease inhibitor tablets. TubR was cleaved overnight from the column using 1 mg of purified SENP (Sentrin/SUMO-specific protease) SUMO protease as described elsewhere (3) and eluted. Peak fractions were pooled for further purification to remove the protease by anion exchange [5 mL HiTrap Q HP, 20 mM Tris·Cl (pH 9), 0.1–1 M NaCl gradient] and size exclusion chromatography [HiLoad Sephacryl S200 16/60, 20 mM Tris·Cl (pH 8.5), 300 mM NaCl, 1 mM EDTA].

Proteins were concentrated before and after size exclusion chromatography in centrifugal concentrators (Merck Millipore) of the appropriate molecular weight cutoff. Typically, TubZ was concentrated up to 20 mg/mL, and TubR was concentrated up to 5 mg/mL. Purified proteins were analyzed using SDS/PAGE [Criterion TGX 4–20% (wt/vol); Bio-Rad], and their concentrations were estimated by a bicinchoninic acid assay (Thermo Scientific). Generally, before the experiments analyzing filament dynamics and nucleation and TubRC transport, TubZ samples were centrifuged again for 10 min at 200,000 × *g* to remove aggregates. After purification and labeling, proteins were aliquoted, flash-frozen in liquid nitrogen, and stored at −80 °C. Initially, an additional cycle of polymerization, centrifugation, and depolymerization during labeling was introduced, but we did not see a significant difference between once-cycled and twice-cycled protein in the microscopy assays; however, losses were significant, so we worked with once-cycled protein for this study.

Indirect Labeling of the TubRC Complex. The centromeric complex TubRC was fluorescently marked by assembling labeled *tubC* DNA and unlabeled TubR at different molecular ratios. For microscopy studies, they were mixed at a ratio of 1:400. The centromeric DNA sequence of pBtoxis *tubC* encompassing iterons 1–7 was amplified by PCR from plasmid pHis17-Bt*tubC* (2), using 5′-biotinylated– or 5′-Atto647NN–conjugated primers (IDT). Before use, the product was gel-purified. A shorter centromeric sequence of *tubC* (iterons 1–3) was produced by annealing primers only and purified in the same manner. Lowercase letters indicate linkers introduced between the dye and *tubC*, and red underlined uppercase letters mark the identified binding sites. Sequences are 5′–3′, starting with iteron 1 and proceeding to iteron 7.

Sequence: Atto647* tubC *1–7. aaataaatAACGGTTTAAATTTAAATTTAATTTTAGGTTTAAATTTCTGGGGGTTATAGAAAGATATATGTATATCTAGTGTGGCTAAAGGTTTAAATAACAGTTTAAATTTAAGTTTAACTTTCAGTTTACATACCATTCCCAGTGTG

Sequence: Atto647* tubC *1–7 biotin. aaataaatAACGGTTTAAATTTAAATTTAATTTTAGGTTTAAATTTCTGGGGGTTATAGAAAGATATATGTATATCTAGTGTGGCTAAAGGTTTAAATAACAGTTTAAATTTAAGTTTAACTTTCAGTTTACATACCATTCCCAGTGTGgggatcccatcatcatcatcattaaaagc

Sequence:* tubC *1–3 Atto647. AACGGTTTAAATTTAAATTTAATTTTAGGTTTAAATTTCTGGGGG

Velocity Analysis. Kymographs were generated using the plug-in by Jens Rietorf and Arne Seitz in ImageJ (NIH) and utilized for velocity analysis. The track of the filament was manually determined using the maximum projection option in ImageJ. Along each trace, a line of three pixels' width was drawn and used to generate the kymograph. Growth and shrinkage velocities for TubZ alone at 150 mM K-glutamate were obtained only from

speckle labeling experiments, except for filaments grown at 320 nM TubZ. Here, only rhodamine-labeled TubZ was used. Only free ends were considered for the analysis, and great care was taken that the minus end shrinking was caused by the loss of subunits. Motion of free *tubC* signals was analyzed at 500 nM and 320 nM TubZ in speckle and nonspeckle experiments at 150 mM K-glutamate.

Quantification of Nucleation Events. Filaments were counted if they started growing as a point like signal, which elongated and then developed into a bar-shaped filament. Afterward, it was checked if a *tubC* signal localized to the attached end. Only the first 5 min after polymerization initiation was considered for filament formation at a low TubZ concentration (320 nM). This time window was shorter at higher TubZ concentrations because filaments quickly covered the surface. The number given in *Results* was obtained using 50 mM K-glutamate and 0.2% methylcellulose at TubZ concentrations ranging from 320 to 800 nM. Data were plotted and analyzed using Prism (GraphPad).

1. Aylett CH, Wang Q, Michie KA, Amos LA, Löwe J (2010) Filament structure of bacterial tubulin homologue TubZ. *Proc Natl Acad Sci USA* 107(46):19766–19771.
2. Aylett CH, Löwe J (2012) Superstructure of the centromeric complex of TubZRC plasmid partitioning systems. *Proc Natl Acad Sci USA* 109(41):16522–16527.
3. van den Ent F, Izoré T, Bharat TA, Johnson CM, Löwe J (2014) Bacterial actin MreB forms antiparallel double filaments. *eLife* 3:e02634.

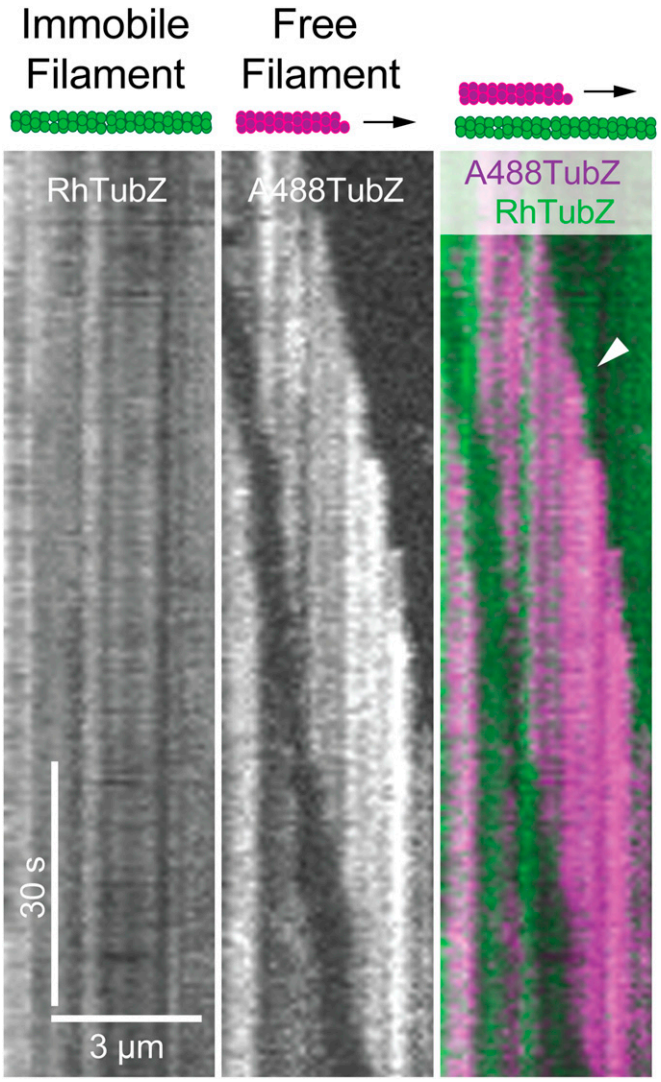

Fig. S1. Filaments treadmilling past each other using each other as a track. Schematic diagrams above the multichannel kymographs illustrate the filaments, and the arrows illustrate the direction of motion. The free A488TubZ filament (magenta) moves from left to right (arrowhead) on top of an immobile green RhTubZ filament. The green RhTubZ filament interacts unspecifically with the surface, something that randomly and occasionally occurred and helped to illustrate the motion of filaments against each other (also Movie S3).

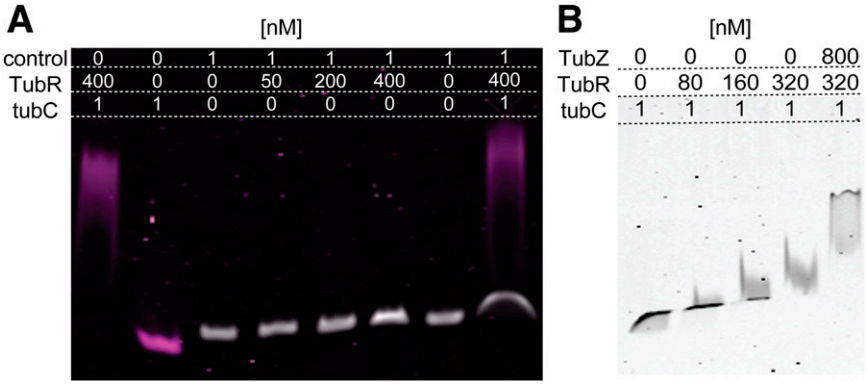

Fig. S2. Specific binding of TubR to *tubC*. (*A*) EMSA of Atto647*tubC* (150 bp, magenta) and an unspecific Atto488-labeled 250-bp DNA fragment (amplified from an ampicillin resistance cassette, white) with TubR protein. Molarities are given above the lanes. Only Atto647*tubC* displays a super shift compared with Atto488DNA, indicative of strong sequence specificity of TubR. (*B*) EMSA of Atto647*tubC*, TubR, and TubZ at different concentrations in medium-salt buffer (150 mM K-glutamate). Atto647*tubC* shifts dependent on the *tubC* input and shows an additional supershift when TubZ is added (last lane).

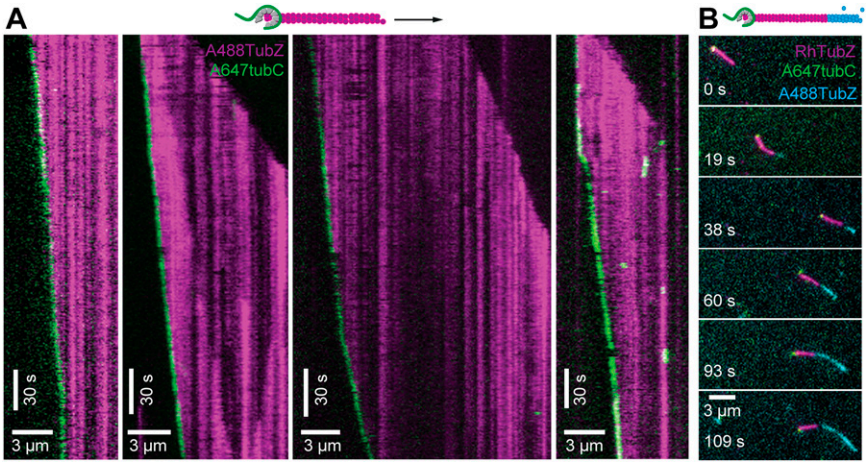

Fig. S3. TubRC tracks the minus end exclusively and not the growing plus end. (*A*) Kymographs of TubRC processively tracking shrinking minus ends. (*Right*) Clearly, TubRC did not follow the growth of TubZ filaments but did also bind laterally along the lattice. However, these events were short-lived compared with processive shrinking minus end tracking. (*B*) Image series of polarity-marked TubZ filament, revealing that TubRC did not drive insertional polymerization. Note that the magenta TubZ filament seed also shortens during the observation from the TubRC-bound end (shortening from 3.13 µm to 1.1 µm).

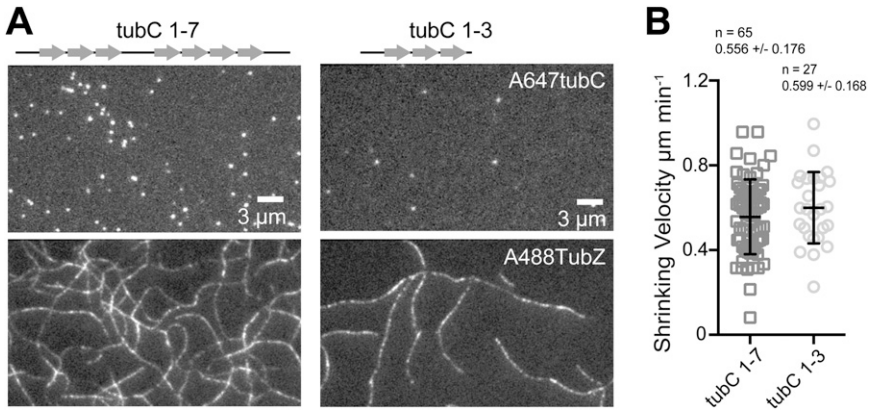

Fig. S4. Filament binding of TubRC using full-length *tubC* (iterons 1–7) and fewer *tubC* iterons (1–3), each labeled with Atto647. (*A*) Images showing recruitment of full-length TubRC (*Top Left*) and TubRC 1–3 (*Top Right*) to TubZ filaments (*Bottom Left* and *Bottom Right*), taken at the same time point after starting the polymerization reaction. The number of bound TubRC filaments is reduced when using truncated *tubC* (1–3). (*B*) Scatter plots comparing shrinking rates of filaments at equimolar ratios of TubR/*tubC* (1–7) (0.556 ± 0.176 μm·min^{-1}, $n = 65$) and TubR/*tubC* (1–3) (0.599 ± 0.168 μm·min^{-1}, $n = 27$; mean ± SD; one experiment). Velocities were similar to full-length *tubC* iterons 1–7, suggesting that *tubC* iterons 1–3 are sufficient to assemble minus end stabilizing centromeric complexes, but the reduced number of minus end-bound TubRC indicated that binding efficiency and possibly filament nucleation are reduced compared with full-length *tubC*. Only 28.1% (32 filaments) carried a persistent signal (defined as not leaving the minus end while observing the TubRC 1–3), whereas 71.4% (42 filaments) carried TubRC (1–7).

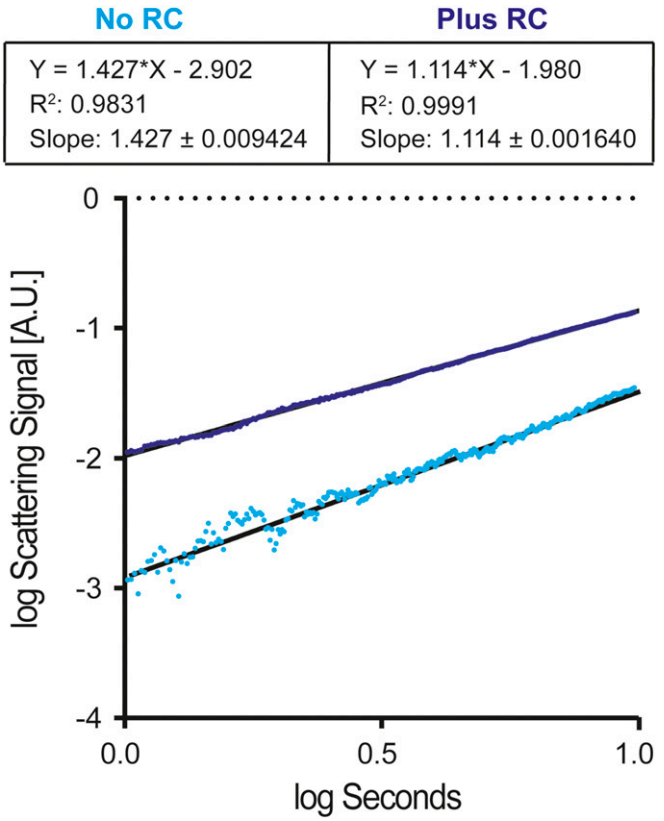

Fig. S5. TubRC reduces the number of steps required for TubZ filament formation. Double logarithmic plot of intensity-normalized light scattering signals during early stages of bulk polymerization experiments. Unlabeled TubZ polymers were formed in the presence or absence of TubRC. Linear regression yielded a difference in slope in the absence and presence of TubRC, with 1.427 ± 0.0094 ($R^2 = 0.98$) vs. 1.114 ± 0.0016 ($R^2 = 0.99$), respectively. TubRC reduced the slope of initial polymerization, indicative of fewer steps for polymer nucleation (1). A.U., arbitrary units.

1. Flyvbjerg H, Jobs E, Leibler S (1996) Kinetics of self-assembling microtubules: An "inverse problem" in biochemistry. *Proc Natl Acad Sci USA* 93(12):5975–5979.

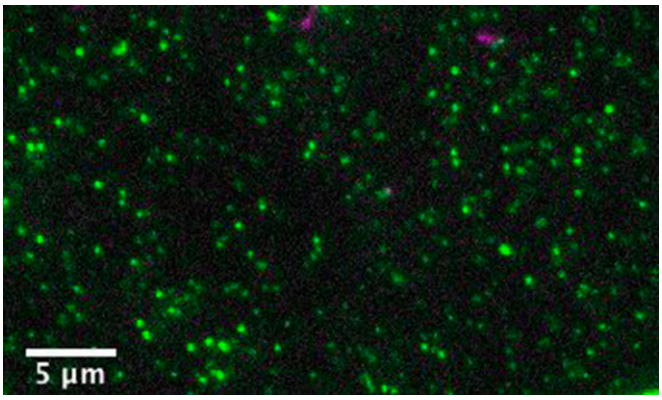

Movie S1. Directed motion by treadmilling TubZ filaments. Labeled green TubZ molecules were inserted sparsely as speckles into magenta filaments. Filaments started moving across the surface directly after initiation of assembly. Treadmilling is easily followed by the polar insertion of green/magenta speckles at growing plus ends and by their loss at the opposite, shrinking minus ends. The movie plays at 20-fold real time.

Movie S1

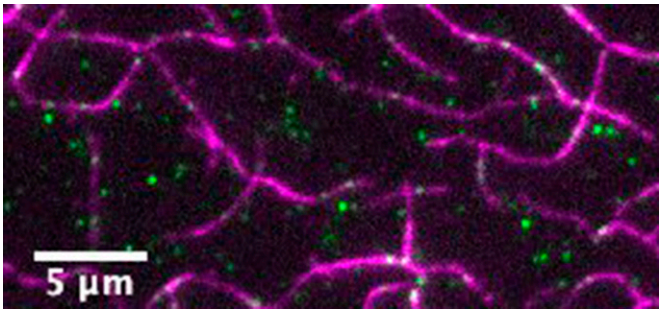

Movie S2. TubZ filaments form a dynamic network. Filaments constantly anneal into bundles and disassemble, driven by the treadmilling dynamics of individual filaments. Separation of bundles depends on their orientation because antiparallel bundles separate, whereas parallel bundles move as a single bundle. The movie plays at 20-fold real time.

Movie S2

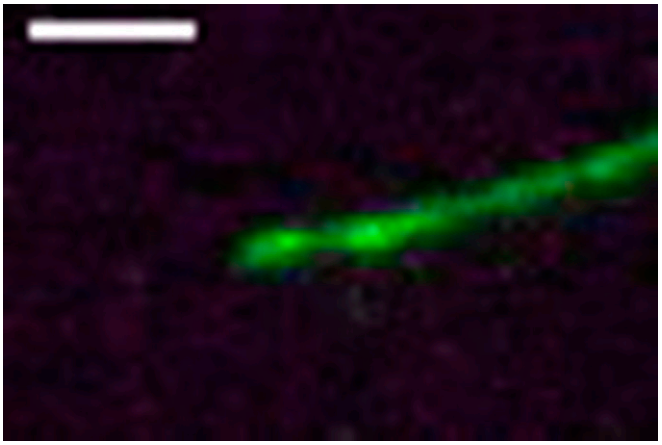

Movie S3. TubZ filaments treadmilling past each other. Free TubZ filaments (magenta) move from right to left along another, immobile TubZ filament (green). Later, a second magenta filament anneals from solution and starts treadmilling along the template filament. The mobile filaments reach the end as they continue treadmilling and start to leave the green filament. The movie plays at 20-fold real time. (Scale bar: 2 µm.)

Movie S3

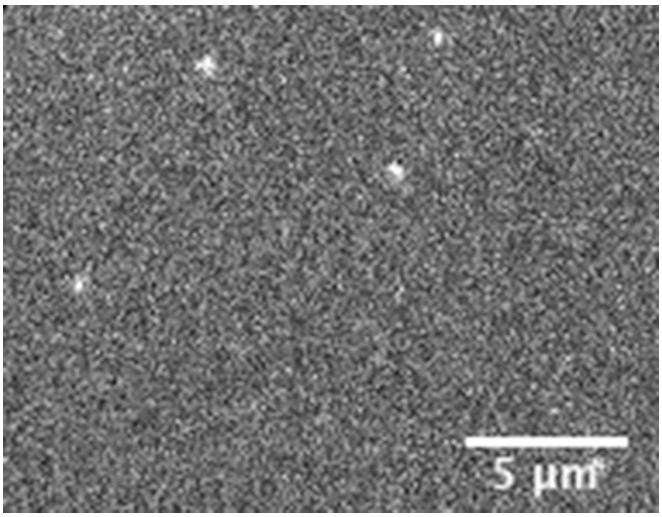

Movie S4. *TubC* motion in the presence of TubZ and TubR. Individual, labeled *tubC* molecules show directed movement across the surface. Motion is only observed in the presence of TubR and TubZ (neither is labeled here). The movie plays at 100-fold real time.

Movie S4

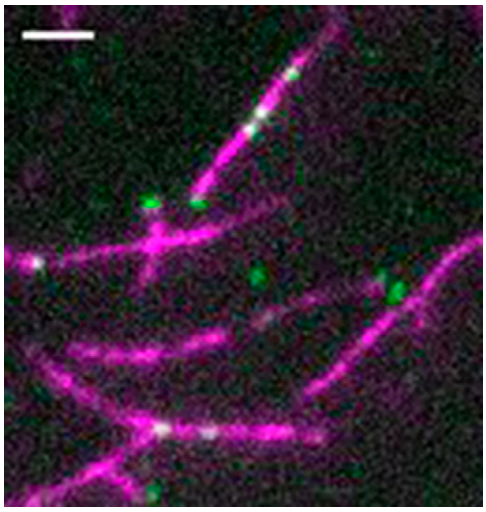

Movie S5. Centromeric TubRC complexes track minus ends processively. TubRC (green) binds to and moves on shrinking minus ends of TubZ filaments (magenta). We never observed TubRC tracking growing plus ends. Some transient lateral binding is also visible, and many such TubRC binding events along the filament length also display directed motility; the directed motility of TubRC on filaments is explained assuming that short filaments treadmill along other TubZ filaments, transporting TubRC until separation of the filaments (as in Movie S3). The movie plays at 40-fold real time. (Scale bar: 2 μm.)

Movie S5

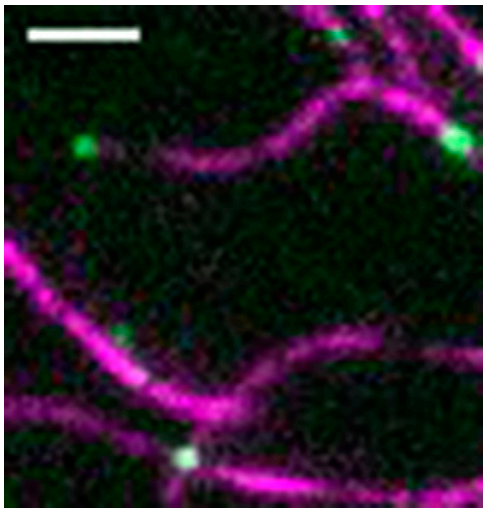

Movie S6. Centromeric TubRC complexes track minus ends processively. This movie illustrates another example of TubRC (green), binding to and tracking shrinking minus ends of TubZ filaments (magenta). The movie plays at 40-fold real time. (Scale bar: 2 μm.)

Movie S6

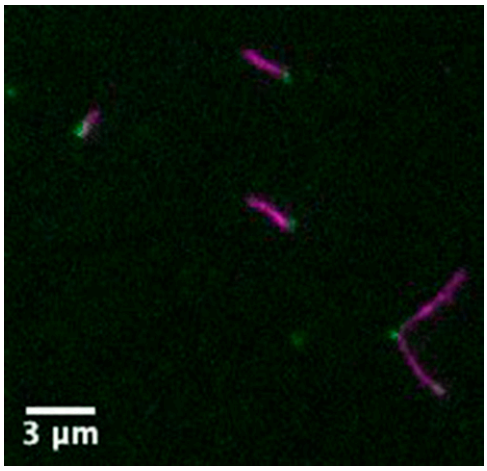

Movie S7. TubZ filament bundles pull centromeric TubRC complexes closer together. Free diffusing TubZ filaments (magenta) emanate from readily assembled and labeled TubRC (green). Filaments anneal by chance, forming bundles (spindles) of different lengths and polarities. In antiparallel arrangements, filaments pull TubRC located at the ends closer together, demonstrating pulling rather than pushing. As in previous movies, some transient lateral association of TubRC complexes with TubZ filaments is visible. The movie plays at 20-fold real time.

Movie S7

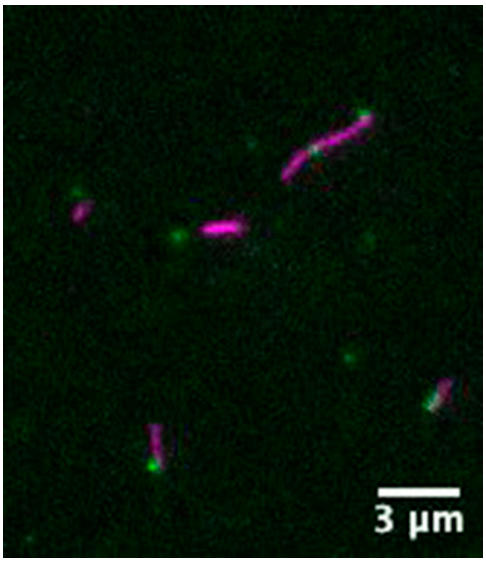

Movie S8. TubZ filament bundles pull centromeric TubRC complexes closer together. This movie illustrates a second example of free diffusing TubZ filaments (magenta) that emanate from readily assembled and labeled TubRC (green). Filaments anneal by chance, forming bundles (spindles) of different lengths and polarities. In antiparallel arrangements, filaments pull TubRC located at the ends closer together, demonstrating pulling rather than pushing. As in previous movies, some transient lateral association of TubRC complexes with TubZ filaments is visible. The movie plays at 20-fold real time.

Movie S8

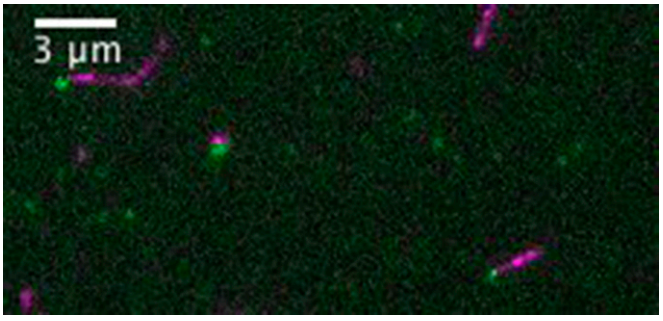

Movie S9. Shorter centromeric *tubC* sequences using *tubC* (1–3) only are sufficient but less efficient for minus end tracking. Compared with Movies S7 and S8, shorter TubRC (green) tracks minus ends of TubZ filaments (magenta). Fewer filament ends are associated with TubRC. The movie plays at 40-fold real time.

Movie S9

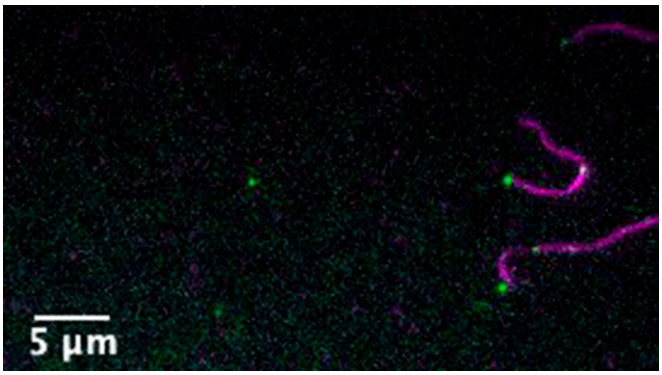

Movie S10. TubRC does not catalyze the addition of TubZ subunits to filaments. Filament seeds (magenta) emanate from (green, minus end) TubRC, whereas TubZ filament extensions grow using differently labeled TubZ (cyan). At equimolar ratios of TubZ to TubRC, cyan extensions are only observed at ends opposite of TubRC; they are hence only extended at the plus end. The motion of the filaments is due to the flow applied to add differently labeled TubZ (cyan). Note that the bottom filament breaks during the flush, forming an antiparallel arrangement (two cyan extensions) in which TuRC molecules move toward each other. The movie plays at 20-fold real time.

Movie S10

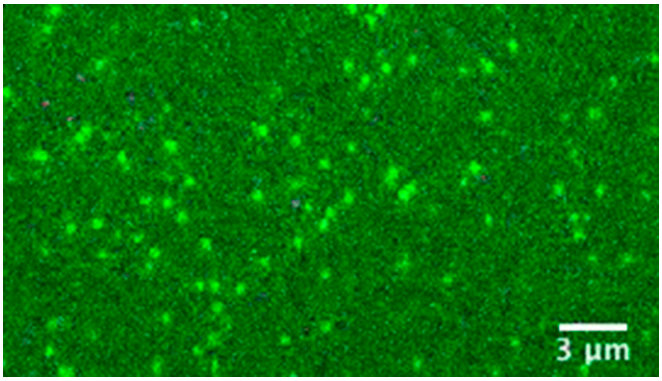

Movie S11. TubZ filament nucleation at immobilized TubRC complexes. At varying TubZ and salt concentrations, filaments (magenta) seed and emanate first from individual (green) TubRC complexes immobilized on the glass surface. Note that short filaments initially swivel, indicating a single attachment site S11 (medium-salt buffer: 0.6% MeCl, 500 nM TubZ, 150 mM K-glutamate). The movie plays at 20-fold real time.

Movie S11

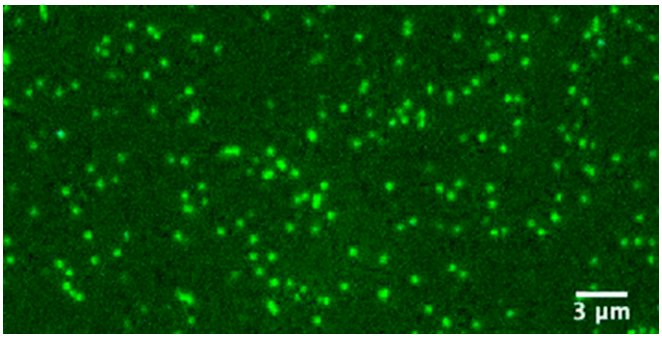

Movie S12. TubZ filament nucleation at immobilized TubRC complexes. At varying TubZ and salt concentrations, filaments (magenta) seed and emanate first from individual (green) TubRC complexes immobilized on the glass surface. Note that short filaments initially swivel, indicating a single attachment site S12 (low-salt buffer: 0.2% MeCl, 320 nM TubZ, 50 mM K-glutamate). The movie plays at 40-fold real time.

Movie S12

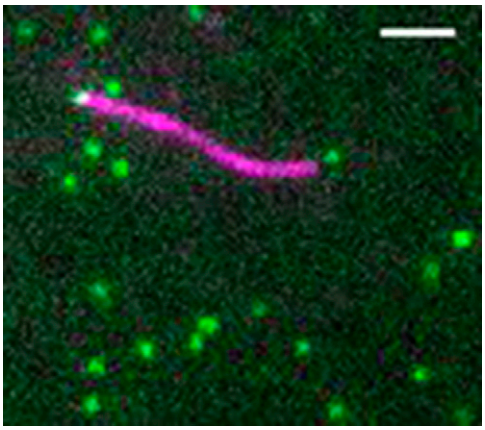

Movie S13. Minus end binding of TubRC stalls TubZ filament movement. A TubZ filament (magenta) treadmills across surface-immobilized TubRC (green). The TubZ filament first adheres to an individual TubRC site, from which it later detaches. Then, it treadmills freely until another TubRC complex (arrowhead) attaches to the free minus end. This movie shows again the persistence of TubRC at the minus end and that binding exerts force by stopping filament movement (but not treadmilling). Speckles leave the filament faster when not bound to TubRC. The movie plays at 20-fold real time. (Scale bar: 2 μm.)

Movie S13